Evaluation by Monte Carlo simulations of the power limits and bit-error rate degradation in wavelength-division multiplexing networks caused by four-wave mixing

Ioannis Neokosmidis, Thomas Kamalakis, Aristides Chipouras, and Thomas Sphicopoulos

Fiber nonlinearities can degrade the performance of a wavelength-division multiplexing optical network. For high input power, a low chromatic dispersion coefficient, or low channel spacing, the most severe penalties are due to four-wave mixing (FWM). To compute the bit-error rate that is due to FWM noise, one must evaluate accurately the probability-density functions (pdf) of both the space and the mark states. An accurate evaluation of the pdf of the FWM noise in the space state is given, for the first time to the authors' knowledge, by use of Monte Carlo simulations. Additionally, it is shown that the pdf in the mark state is not symmetric as had been assumed in previous studies. Diagrams are presented that permit estimation of the pdf, given the number of channels in the system. The accuracy of the previous models is also investigated, and finally the results of this study are used to estimate the power limits of a wavelength-division multiplexing system. © 2004 Optical Society of America

OCIS codes: 060.4230, 190.4380.

1. Introduction

Wavelength-division multiplexing (WDM) is a promising technology for the achievement of all-optical networks that permits the full utilization of the fiber bandwidth. However, the performance of a WDM system is strongly influenced by both linear and nonlinear phenomena that determine the signal propagation inside the optical fiber. Although linear propagation effects may be compensated for by optical amplifiers and chromatic dispersion compensators, there is a class of nonlinear effects such as self-phase modulation, cross-phase modulation, and four-wave mixing (FWM) that pose additional limitations in dense WDM systems. Both cross-phase modulation and FWM cause interference between channels of different wavelengths, resulting in an upper power limit for each WDM channel. However, the most severe problems are imposed by FWM because the power of the FWM product is inversely proportional to the square of the channel spacing, whereas the influence of cross-phase modulation is approximately inversely proportional to the channel spacing.[1,2]

In this paper an accurate statistical description of FWM noise is given, and its influence on system performance is investigated. The properties of FWM noise are investigated by use of numerical Monte Carlo simulations for both the mark and the space states. The results show that in the space state the probability-density function (pdf) of FWM–FWM beating noise, which constitutes the main noise source of the system, exhibits exponential decay. The computed pdf for the mark state is shown to be asymmetric, a fact that is confirmed theoretically as well. Estimations of the pdf for the mark and the space states are accomplished with relevant diagrams in terms of the number of channels within the system.

A comparison of the values of the error probabilities obtained by the present method and by two other methods previously proposed[3,4] is carried out. In the first of the previous methods, Gaussian statistics for the FWM noise in the optical domain are assumed, permitting the computation of the system's

The authors are with the Department of Informatics and Telecommunications, University of Athens, Panepistimiopolis Ilissia, Athens GR-15784, Greece. I. Neokosmidis's e-mail address is i.neokosmidis@di.uoa.gr.

Received 15 December 2003; revised manuscript received 13 May 2004; accepted 7 June 2004.

0003-6935/04/265023-10$15.00/0

bit-error rate (BER) in closed form.[3] Although this approach might provide a first insight into the implications of the FWM noise, its validity must be examined because the assumption of Gaussian statistics is somewhat arbitrary. Indeed, FWM noise is the sum of a large number of components that depend on one another. Hence the central-limit theorem,[5] on which the Gaussian approximation is based, may not be valid in this case. In the other previous approach the pdf of the FWM noise in the mark state can be approximated with a symmetrical double-sided exponential distribution.[4] However, as was mentioned above, the distribution of the FWM noise in the mark state is asymmetric and hence the symmetrical exponential approximation may prove inaccurate. It is shown that, in many cases, there are significant differences between the two approaches. Finally, the proposed model is used to assess the implications of FWM in a WDM system that employs nonzero dispersion or standard single-mode fibers as well.

The rest of the paper is organized as follows: In Subsection 2.A some basic considerations are given concerning the origin of the FWM phenomenon, which are used in Subsection 2.B to derive an expression for the photocurrent at the receiver. This expression is used in Section 3 to compute numerically the pdfs of the FWM noise in the mark and space states. Also, the asymmetry of the pdf in the mark state as observed in the simulations is theoretically justified. The accuracy of the symmetrical double-sided pdf is investigated in Subsection 4.A, and the validity of the Gaussian approximation is examined in Subsection 4.B. The implications of the FWM effect in a WDM system are discussed in Section 5. In Section 6, guidelines for the incorporation of the other noises [thermal and amplified spontaneous emission (ASE)] are given. Our research is summarized in Section 7.

2. Basic Assumptions and Theoretical Background

A. Four-Wave Mixing

A WDM system with equally spaced channels and amplitude-shift keying modulation, which is the most frequently used modulation scheme is considered here. All signals are assumed to be copolarized and synchronized, which represents a worst-case situation.[6] Only the pdf of the photocurrent for the central channel has to be derived for the calculation of the BER because, in this case, the energy-conservation requirement is satisfied by the largest number of frequency combinations.[7] Provided that the photocurrent depends on the bit values and on the optical phases of all channels in a rather complicated random manner, a closed form of the pdf of the FWM noise is not possible. Consequently, Monte Carlo (MC) simulations are used for its determination.

The origin of the FWM effect is the existence of the third-order nonlinear polarization vector $\mathcal{W}_{\mathrm{NL}}$. Considering optical waves oscillating at frequencies ω_i and linearly polarized along the same axis x, $\mathcal{W}_{\mathrm{NL}}$ is expressed in the following form:

$$\begin{aligned}\mathcal{W}_{\mathrm{NL}} &= \hat{x}\tfrac{1}{2} \sum \mathcal{W}_i \exp[j(k_i z - \omega_i t)] + \text{c.c.} \\ &= \hat{x}\tfrac{1}{2} \sum \mathcal{W}_i \exp(j\theta_i) + \text{c.c.},\end{aligned} \tag{1}$$

where $\mathcal{W}_i$ is the amplitude of the third-order polarization at frequency ω_i. For $i = n$, where n is the assumed channel, it can be shown that[8]

$$\begin{aligned}\mathcal{W}_n = \frac{3\varepsilon_o}{4}\chi^{(3)}_{xxxx}|E_n|^2E_n + \frac{3\varepsilon_o}{4}\chi^{(3)}_{xxxx}\sum_{pqr}[2(|E_p|^2 + |E_q|^2 \\ + |E_r|^2)E_n] + \frac{3\varepsilon_o}{2}\chi^{(3)}_{xxxx}\sum_{pqr}E_pE_qE_r^* \exp[j(\theta_p \\ + \theta_q - \theta_r - \theta_n)] + \ldots,\end{aligned} \tag{2}$$

where E_i is the electric field at frequency ω_i, ϵ_o is the vacuum permittivity, and $\chi^{(3)}_{xxxx}$ is the third-order nonlinear susceptibility. The third sum is the contribution of FWM noise. This sum runs for all integers p, q, and r that satisfy the conditions $p + q - r = n$ (which is imposed by the energy-conservation requirement) and $r \neq p, q$ (which guarantees that the corresponding term is not due to self- or cross-phase modulation).

The output power P_{pqr} of the FWM product is given by[9]

$$P_{pqr} = \frac{\gamma^2}{9} d_{pqr}{}^2 P_p P_q P_r \exp(-aL) L_{\mathrm{eff}}{}^2 \eta, \tag{3}$$

where P_i ($i = p, q, r$) represents the input peak power at frequencies $f_i = \omega_i/2\pi$ in the mark state. Assuming a perfect extinction ratio, the average input power is $P_{\mathrm{av}} = P_i/2$. It should be noted that Eq. (3) is an approximation that holds because the power of the FWM components is quite small compared with each channel's power.[10] In a WDM system it can be assumed that all the peak powers at the mark state are equal ($P_i = P_{\mathrm{in}}$ for $i = 1, 2, \ldots, N$). In Eq. (3) γ is the nonlinear coefficient of the fiber,[9] a is the fiber loss coefficient, L is the total fiber length, $L_{\mathrm{eff}} = [1 - \exp(-aL)]/a$ is the effective length of the fiber, d_{pqr} is the degeneracy factor ($d_{pqr} = 3$ when $p = q$, $d_{pqr} = 6$ when $p \neq q$), and η is the mixing efficiency, given by

$$\eta = \frac{a^2}{a^2 + (\Delta\beta)^2}\left\{1 + \frac{4\exp(-aL)\sin^2(\Delta\beta L/2)}{[1 - \exp(-aL)]^2}\right\}. \tag{4a}$$

In Eq. (4a), $\Delta\beta$ represents the phase mismatch and may be expressed in terms of channel frequencies f_i:

$$\begin{aligned}\Delta\beta &= \frac{2\pi\lambda^2}{c}(f_p - f_r)(f_q - f_r)\left\{D(\lambda_o) + \frac{dD(\lambda_o)}{d\lambda}\left(\frac{\lambda^2}{2c}\right)\right. \\ &\quad \left.\times[(f_p - f_o) + (f_q - f_o)]\right\} \\ &= \frac{2\pi\lambda^2}{c}\Delta f^2(p - r)(q - r)\left\{D(\lambda_o)\right. \\ &\quad \left. + \frac{dD(\lambda_o)}{d\lambda}\left(\frac{\lambda^2}{2c}\right)\Delta f[(p - o) + (q - o)]\right\},\end{aligned} \tag{4b}$$

or, approximately,

$$\Delta\beta \approx \frac{2\pi\lambda^2 D}{c}\,\Delta f^2(p-r)(q-r). \tag{4c}$$

In Eq. (4b), D is the fiber's chromatic dispersion coefficient, λ is the wavelength of the signal, and c is the speed of light in vacuum. Expression (4c) is derived from the fact that, for typical values of D, $dD/d\lambda$, and Δf, the term involving $dD/d\lambda$ is small.[4]

Unlike in previous studies, the statistics of the space state are also considered. The amplitudes of the optical fields, $E^{(m)}$ and $E^{(s)}$ in the mark and the space states, respectively, at a given channel n are written as[3]

$$E^{(m)} = \sqrt{P_n \exp(-aL)}\,\exp(j\theta_n) + \sqrt{P_{F(\mathrm{IM})}{}^{(m)}}\,\exp[j\theta^{(m)}_{F(\mathrm{IM})}](\mathrm{mark}), \tag{5a}$$

$$E^{(s)} = \sqrt{P_{F(\mathrm{IM})}{}^{(s)}}\,\exp[j\theta^{(s)}_{F(\mathrm{IM})}](\mathrm{space}), \tag{5b}$$

where P_n and θ_n are the input peak power and the phase in the mark state, respectively, of given channel n

$$\sqrt{P^{(m)}_{F(\mathrm{IM})}}\,\exp[j\theta^{(m)}_{F(\mathrm{IM})}] = \sum_{p\neq q\neq r\neq n} B_pB_qB_r\sqrt{P_{pqr}}\times\exp(j\theta_{pqr}) + \sum_{p\neq q\neq r=n} B_pB_q\sqrt{P_{pqn}}\times\exp(j\theta_{pqn}) + \sum_{p=q\neq r} B_pB_r\sqrt{P_{ppr}}\times\exp(j\theta_{ppr}), \tag{6a}$$

$$\sqrt{P^{(s)}_{F(\mathrm{IM})}}\,\exp[j\theta^{(s)}_{F(\mathrm{IM})}] = \sum_{p\neq q\neq r\neq n} B_pB_qB_r\sqrt{P_{pqr}}\times\exp(j\theta_{pqr}) + \sum_{p=q\neq r} B_pB_r\sqrt{P_{ppr}}\times\exp(j\theta_{pqr}), \tag{6b}$$

whereas P_{pqr} and $\theta_{pqr} = \theta_p + \theta_q - \theta_r$ are the peak power and the phase, respectively, of the FWM noise generated from a channel combination (p, q, r). Furthermore, $B_i = 0$ or $B_i = 1$ is the bit value of channel i. These expressions for the electric field are used in Subsection 2.B to derive an expression for the photocurrent at the receiving photodiode.

B. Calculation of the Photocurrent

At the receiver, the photocurrent is proportional to the optical power and hence to $|E|^2$, where $E = E^{(m)}$ or $E = E^{(s)}$.[11] In practical applications it can be assumed that $\Delta\beta \gg a$, which generally holds for $D \geq 2$ (ps/nm)/km and channel spacing $\Delta f \geq 10$ GHz. For large L, one can also use the fact that $\exp(-aL) \ll 1$. Assuming a single fiber span without optical amplification, all other noises at the receiver except for FWM can be ignored. This is especially true for high input powers, and in this case the photocurrent at the detector is written as

$$S^{(m)} = k|E^{(m)}|^2 \approx kP_n\exp(-aL) + 2k\delta\sqrt{P_n\exp(-aL)}\,I_m, \tag{7a}$$

$$S^{(s)} = k|E^{(s)}|^2 \approx k\delta^2 I_s, \tag{7b}$$

where k is the receiver's responsivity and

$$\delta = \frac{\gamma c}{2\pi\lambda^2 D\Delta f^2}\,P_{\mathrm{in}}{}^{3/2}\exp(-aL/2), \tag{8a}$$

$$I_m = \frac{1}{3}\sum_{pqr} B_pB_qB_r\,\frac{d_{pqr}}{|p-n||q-n|}\cos(\theta_{pqr}-\theta_n), \tag{8b}$$

$$I_s = \left(\frac{1}{3}\sum_{\substack{pqr\\ r\neq n}} B_pB_qB_r\,\frac{d_{pqr}}{|p-n||q-n|}\cos\theta_{pqr}\right)^2 + \left(\frac{1}{3}\sum_{\substack{pqr\\ r\neq n}} B_pB_qB_r\,\frac{d_{pqr}}{|p-n||q-n|}\sin\theta_{pqr}\right)^2. \tag{8c}$$

Formulas (7a) and (7b) provide expressions for the photocurrent in the mark and the space states in terms of two new variables, I_m and I_s, given by Eqs. (8b) and (8c), respectively. It is interesting to note that, for a given number of channels, these new variables depend only on the bits and the phases of the optical signals.

3. Statistical Behavior of Photocurrents $S^{(m)}$ and $S^{(s)}$: Computation of the pdf by Monte Carlo Simulation

In this section the pdfs of I_m and I_s are computed by MC simulations. The optical phases of all channels are assumed to be uniformly distributed within $[0, 2\pi]$ because of phase noise,[11] and the data bits are assumed to be in the mark and the space states with equal probability, $P(B_i = 0) = P(B_i = 1) = 1/2$. Hence the statistics of I_m and I_s will depend only on the total number of channels N and on channel number n, which is assumed to be the central channel: $n = \lceil N/2 \rceil$. Variables I_m and I_s are related to the optical phases and to the values of the optical bits in a rather complicated manner, and consequently their pdf cannot be derived in closed form. To obtain the pdfs of I_m and I_s through which the pdfs of $S^{(m)}$ and $S^{(s)}$ will be determined, we performed a series of ν MC experiments. $\nu = 10^{11}$ for $N = 8$, 16 channels, and $\nu = 10^{10}$ for $N = 32$ channels (because of the increased computation time required). The results obtained for the space and the mark states are plotted in Figs. 1(a) and 1(b), respectively.

It is easily deduced that in all cases the pdf exhibits an almost exponential behavior of the form $y = Ae^{bx}$ [solid curves in Figs. 1(a) and 1(b)]. Specifically, the

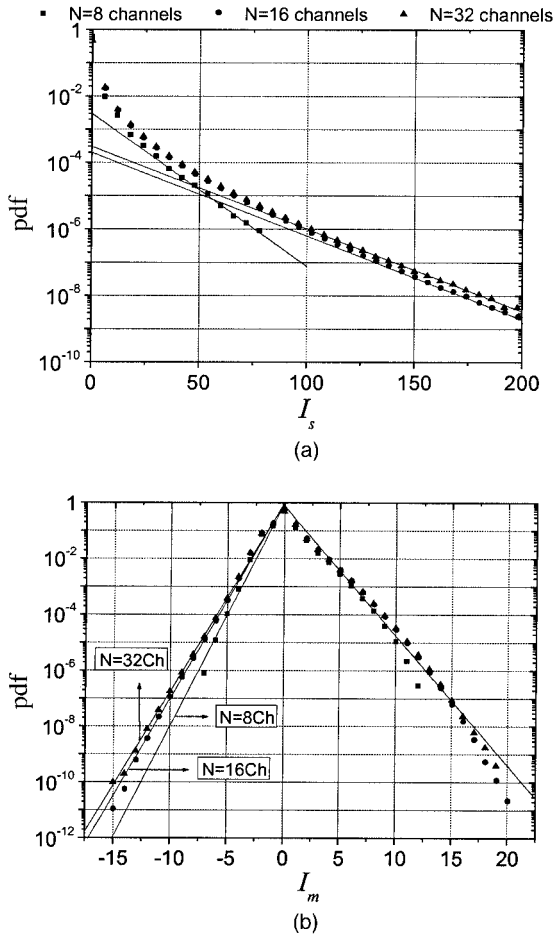

Fig. 1. Pdfs of (a) the space and (b) the mark states. The exponential fittings for the pdfs are shown by solid curves.

pdf in the space state follows an exponential decay, whereas in the mark state the pdf can be approximated by an asymmetrical double-sided exponential distribution. Hence the exponential approximation can be used away from $I_{s,m} = 0$, in the region of the tails, to provide an accurate estimation for the pdfs. To evaluate parameters A and b with respect to N, we performed a series of MC experiments for various values of $N < 32$. The values of parameters A and b calculated for each N are shown in Figs. 2(a)–2(d). To reduce the number of parts of Fig. 2, parameter A is taken equal to the peak of the pdf of I_m and is the same for $I_m > 0$ and $I_m < 0$. Given this value of A, the value of b for $I_m > 0$ is calculated such that the exponential Ae^{bx} approximates the tails at the right of the pdf. The same is done for $I_m < 0$. For the pdf of I_s, parameters A and b are calculated such that the tail of the pdf of I_s is accurately approximated. As shown in Figs. 2(a)–2(d), A and b exhibit an approximate $y_0 + y_1 \exp(-N/t)$ dependence. The values of y_0, y_1, and t in each case are given in the figures. Given the number of channels N, Figs. 2(a)–2(d) are useful in determining A and b for the mark and the space states, and consequently the shapes of the pdfs of I_m and I_s, without the need to perform MC simulations. For $N > 32$, parameters A and b do not vary significantly; hence their values obtained for $N = 32$ can be used.

Once the pdfs of I_m and I_s are determined, the pdfs of $S^{(m)}$ and $S^{(s)}$ can also be determined, by use of the theorem of transformation of random variables.[5] Applying this theorem and using relations (7a) and (7b) yield

$$f_{S^{(m)}}[S^{(m)}] = \frac{1}{2k\delta\sqrt{P_n \exp(-aL)}} f_{I_m} \times \left[\frac{S^{(m)} - kP_n \exp(-aL)}{2k\delta\sqrt{P_n \exp(-aL)}}\right], \quad (9a)$$

$$f_{S^{(s)}}[S^{(s)}] = \frac{1}{k\delta^2} f_{I_s}\left[\frac{S^{(s)}}{k\delta^2}\right], \quad (9b)$$

where f_X is the pdf of the variables $X = I_m, I_s, S^{(m)}$ and $S^{(s)}$, respectively. Hence, given the number of channels N in the system, the pdfs of I_m and I_s can be determined from Figs. 2(a)–2(d). The computation of the pdfs of $S^{(m)}$ and $S^{(s)}$ can then be carried out with expressions (7a) and (7b). These pdfs are used in the following sections to estimate the performance of the system.

From Fig. (1b) it can be seen that the pdf for the mark state is not symmetric about $x = 0$. To justify the asymmetry of the pdf, the odd-order moments $\langle I_m^{2u+1}\rangle = \int_{-\infty}^{+\infty} x^{2u+1} f_{I_m}(x)\mathrm{d}x$ of I_m can be examined. If one of the odd-order moments is nonzero, then pdf $f_{I_m}(x)$ is not symmetric. Indeed, if $f_{I_m}(x)$ were symmetric about $x = 0$, then the product of odd function x^{2u+1} and f_{I_m} would be an odd function of x for every integer u; hence the integral of $x^{2u+1} f_{I_m}$ from $-\infty$ to ∞, which gives $\langle I_m^{2u+1}\rangle$, would be equal to zero. Therefore, to show that f_{I_m} is not symmetric it is sufficient to show that there exists one u for which $\langle I_m^{2u+1}\rangle \neq 0$.

As it can be seen from Appendix A, it is easy to expand the terms of the odd-order moments into a positive linear superposition of terms of type $\cos\theta$, whose mean value is either 1 if $\theta \equiv 0$ or 0 if $\theta \neq 0$. Following the method described above, one can obtain $\langle I_m\rangle = 0$ for $u = 0$ and $\langle {I_m}^3\rangle > 0$ for $u = 1$. Hence, at least one odd moment of I_m is nonzero, and it can be concluded that the pdf of I_m is asymmetric. Because both the symmetric exponential and the Gaussian pdf are even functions, they may not provide an accurate description for the statistical behavior of I_m, as is further illustrated in the next sections.

4. Comparison with Other Models

A. Symmetrical Exponential pdf Approximation

One can demonstrate the difference between the symmetrical exponential approximation and the numerically computed pdf by calculating the probability P_{e1} that an error occurs in the mark state, which is written as

$$P_{e1} = \int_{-\infty}^{Q} f_{S^{(m)}}(\xi)\mathrm{d}\xi, \quad (10)$$

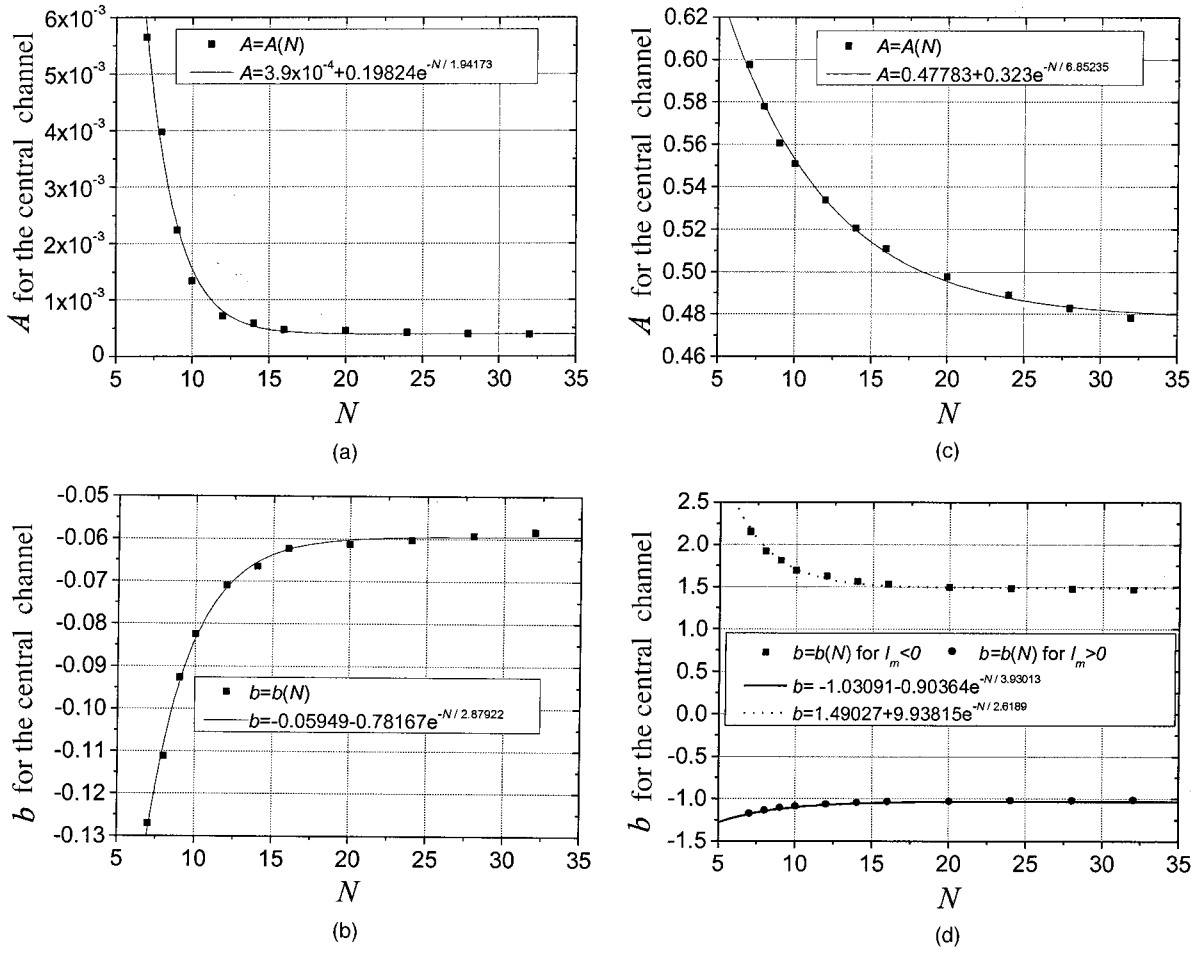

Fig. 2. (a), (b) Parameters A and b in the space state for the central channel with respect to the number of channels N. (c), (d) Parameters A and b in the mark state for the central channel with respect to the number of channels N.

where Q is the receiver decision threshold. The pdf $f_{S^{(m)}}$ of the photocurrent $S^{(m)}$ in the mark state can be evaluated from Eq. (9a) by use of the symmetrical exponential approximation[4] for the pdf:

$$f_{\exp}(I_m) = \frac{1}{\sqrt{2}\sigma} \exp\left(\frac{-\sqrt{2}|I_m|}{\sigma}\right), \tag{11}$$

where σ^2 is the noise variance of I_m given in Ref. 4. We have chosen to compute P_{e1} and not the average BER because in Ref. 4 no pdf was given for the space state that permits the direct computation of error probability P_{e0} in this state.

In the remainder of this paper the parameters used in the calculations are as follows: $\lambda = 1.55$ μm, $c = 3 \times 10^8$ m/s, $L = 80$ km, $a = 0.2$ dB/km, $\gamma = 2.4(\text{km} \times \text{W})^{-1}$, and $k = 1.28$ A/W.

Figure 3(a) shows the pdf of the photocurrent for $N = 16$, $D = 10$ (ps/nm)/km, $P_{\text{in}} = 5$ dBm, and $\Delta f = 25$ GHz and gives a first glance at the effectiveness of the symmetrical exponential approximation in describing the statistics of the photocurrent. It should be noted that only the left-hand part of the pdf is shown in the figure. This happens because, for practical values of the BER, one needs only this part of the pdf to compute P_{e1} from Eq. (10). In Figs. 3(b) and 3(c), P_{e1} is plotted as a function of the receiver threshold for $N = 16$, $D = 10$ (ps/nm)/km, $P_{\text{in}} = 5$ dBm, and $\Delta f = 25$ GHz and for $N = 8$, $D = 5$ (ps/nm)/km, $P_{\text{in}} = 18$ dBm, and $\Delta f = 100$ GHz, respectively. For the numerically calculated pdfs, P_{e1} was computed by numerical integration of Eq. (10). In Figs. 3(b) and 3(c) there is an obvious deviation between the two models, which is several orders of magnitude in the cases examined and implies that the average BER will be much higher for the exponential approximation. For example, as shown in Fig. 3(b), for a threshold $Q = 60$ μA the values of P_{e1} are 2×10^{-5} and 7×10^{-7} for the symmetrical exponential pdf and the numerically computed pdf, respectively. Hence it is evident that the symmetrical exponential model may overestimate the system's BER by ~2 orders of magnitude for error probabilities of the order of 10^{-9}. However, it can easily be used to estimate an upper bound of the BER.

To further illustrate the difference between the symmetrical exponential and the numerically computed pdf, we have plotted in Fig. 3(d) the values of σ obtained for a symmetrical exponential pdf, using the

closed-form formula of Ref. 4 (solid curves). Also plotted are the values of σ' obtained by fitting the numerical pdf with $1/\sigma'/2^{1/2}\exp(2^{1/2}I_m/\sigma')$ for $I_m < 0$. As one can observe from the figure, there is some difference between the values of σ and σ', and this is a further indication that the symmetrical exponential pdf fails to describe the statistical behavior of I_m. It should also be noted that Fig. 3(d) provides an alternative approximation for the numerically computed pdf of I_m for $I_m < 0$. Once the value of σ' is obtained from Fig. 3(d), one can use the pdf of Ref. 4 [i.e., Eq. (11)] to approximate the pdf for $I_m < 0$ by replacing σ with σ'.

B. Gaussian pdf Approximation

The most common approach to the calculation of the BER in the presence of FWM is to assume that the FWM noise is Gaussian. According to the Gaussian approximation[3] the error probability is written as

$$P_e = \frac{1}{\sqrt{2\pi}}\int_{Q_g}^{\infty}\exp\left(-\frac{t^2}{2}\right)\mathrm{d}t = \frac{1}{2}\,\mathrm{erfc}\left(\frac{Q_g}{\sqrt{2}}\right), \quad (12)$$

where Q_g is the Q factor, given by

$$Q_g = \frac{\langle S^{(m)}\rangle - \langle S^{(s)}\rangle}{\sigma^{(m)} + \sigma^{(s)}} \approx \frac{kP_n\exp(-aL) - k\left(\frac{1}{8}\sum_{p\neq q\neq r\neq n}P_{pqr} + \frac{1}{4}\sum_{p=q\neq r}P_{ppr}\right)}{\left(2k^2P_n\exp(-aL)\left\{\frac{1}{8}\sum_{p\neq q\neq r\neq n}P_{pqr} + \frac{1}{4}\sum_{p\neq q\neq r=n}P_{pqn} + \frac{1}{4}\sum_{p=q\neq r}P_{ppr}\right)^{1/2}}. \quad (13)$$

To compute the value of the BER obtained by the actual pdfs of $S^{(m)}$ and $S^{(s)}$ the following formula is used:

$$P_e = \frac{1}{2}\int_{Q}^{\infty} f_{S^{(s)}}(\xi)\mathrm{d}\xi + \frac{1}{2}\int_{-\infty}^{Q} f_{S^{(m)}}(\xi)\mathrm{d}\xi, \quad (14)$$

where the first and second terms are the probabilities that an error will occur in the space and the mark states, respectively, whereas decision level Q is chosen such as to minimize error probability P_e. This computation can be made by solution of the equation $\mathrm{d}P_e/\mathrm{d}Q = 0$, using well-known numerical methods.

The accuracy of the Gaussian approximation in predicting P_{e1} and the BER is examined in Fig. 4(a) for $N = 16$, $D = 10$ (ps/nm)/km and $\Delta f = 25$ GHz and in Fig. 4(b) for that case and for $N = 32$, $D = 15$ (ps/nm)/km, and $\Delta f = 10$ GHz.

From Fig. 4 it is evident that the Gaussian model cannot be used to estimate the BER accurately. The error in the estimation of the BER is more pronounced for small error rates ($<10^{-9}$). For example, for $P_{\mathrm{in}} = 2$ dBm, $P_e = 10^{-18}$ for the Gaussian approximation and $P_e = 10^{-5}$ in the numerically calculated case shown in Fig. 4(b).

The results of Fig. 4 are obtained when $D \geq 2$ (ps/nm)/km. If the WDM system operates near the zero-dispersion wavelength the formulation of formulas (7) and Eqs. (8) is not applicable. To investigate the validity of the Gaussian approximation in such systems, one must estimate the pdfs of photocurrents $S^{(m)}$ and $S^{(s)}$ through MC simulations, applying $S^{(m)} = k|E^{(m)}|^2$ and $S^{(s)} = k|E^{(s)}|^2$, where $E^{(m)}$ and $E^{(s)}$ are given by Eqs. (5) and (6) and P_{pqr} is obtained by use of Eqs. (3), (4a), and (4b), with $D = 0$ [note that formula (4c) does not apply in this case]. The results obtained by the MC simulations (filled circles) and the Gaussian approximation (curves) when $D = 0$ (for the central channel) are illustrated in Fig. 5 for $N = 16$ channels, $P_{\mathrm{in}} = 0$ dBm, $\mathrm{d}D/\mathrm{d}\lambda = 0.07$ (ps/nm^2)/km, and $\Delta f = 100$ GHz. Inspecting Fig. 5, one can understand that, even though the difference between the pdfs of the present and the Gaussian models are reduced in the mark state, they remain observable because the FWM products are correlated and the central-limit theorem is not valid in this case as well.

5. Estimation of Power Limits That Are Due to Four-Wave Mixing

In practice, to evaluate the performance of the system it is useful to have a relation between the BER and the input power. With the method presented here it is quite easy to calculate the BER by using numerical integration, given the characteristics of the system. Once the BER is determined, one may calculate other useful system performance measures such as the packet error rate in Internet Protocol over WDM systems.[12]

Figures 6(a)–6(c) depict the variations of the BER with respect to the variations of the channel spacing, the signal power, and the fiber chromatic dispersion in a dense WDM system. The error probability was calculated by numerical integration of Eq. (14). For calculations of the BER, the optimum decision threshold, i.e., the threshold that minimized the error probability P_e, was chosen. Figure 6 shows that P_e tends to diminish rapidly below a certain power value. This happens because, inasmuch as $|\cos\theta| \leq 1$, random variables $|I_m|$ and I_s cannot exceed a certain value $I_{m,\max}$ and $I_{s,\max}$ obtained by setting $\theta_i = 0$ and $B_i = 1$ in Eqs. (8b) and (8c), respectively. Hence for low input powers the distributions of the mark and space states may not overlap at all, which implies error-free transmission.[13] However, in practical systems the existence of other noises (e.g., thermal noise) will force the two distributions to overlap, preventing the BER from becoming zero.

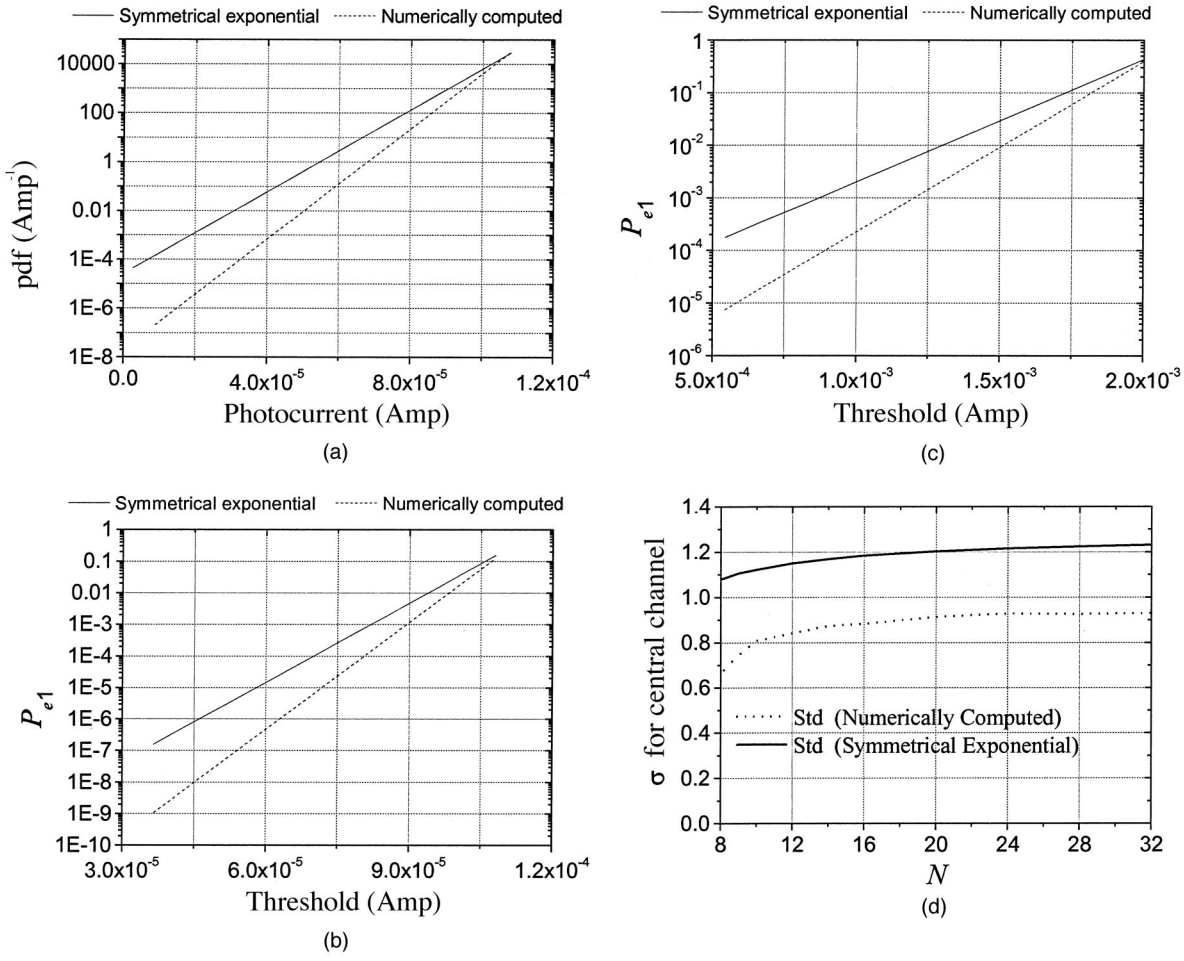

Fig. 3. (a) pdf of the photocurrent for $N = 16$, $D = 10$ (ps/nm)/km, $P_{\text{in}} = 5$ dBm, and $\Delta f = 25$ GHz. (b) Error probability P_{e1} for the mark state with respect to the receiver threshold for the same parameters. (c) P_{e1} as a function of receiver threshold for $N = 8$, $D = 5$ (ps/nm)/km, $P_{\text{in}} = 18$ dBm, and $\Delta f = 100$ GHz. (d) Standard deviation of the sum I_m for the central channel with respect to the number of channels N for the symmetrical distribution and the numerically computed distribution.

When the dispersion or the channel spacing is increased, lower values of P_e are achieved at a given input power. This result can be explained by Eqs. (4a) and (4b), which give mixing efficiency η and phase mismatch $\Delta\beta$. From these equations it is easy to see that the mixing efficiency increases when dispersion D, channel spacing Δf, or both are reduced. As power P_{pqr} of the FWM product given by Eq. (3) is proportional to mixing efficiency η, it is expected that the noise power will be increased and that the performance of the system will degrade. Similar behavior is observed when the number of channels is reduced. This takes place because the number of neighboring channels on each side of the central channel is reduced and, therefore, the number of channel combinations (p, q, r) that satisfy the condition $p + q - r = n$ is also reduced. Hence the power of the FWM noise will decrease when the number of channels is decreased. It is interesting to note that an increase in the number of channels above a certain value does not significantly change the system's performance. For example, for $D = 5$ (ps/nm)/km, $\Delta f = 25$ GHz, and $P_{\text{in}} = 4.5$ dBm, a BER of 10^{-9} is achieved for $N = 8$ channels, a BER of 7×10^{-7} is achieved for $N = 16$ channels, and a BER of 10^{-6} is achieved for $N = 32$ channels. This happens because these channels, which are far from the central channel, do not play a significant role in the production of the FWM noise.

From Figs. 6(a)–6(c) it is confirmed that a simple way to eliminate the effects of FWM is to use nonzero-dispersion fibers and WDM systems with large channel spacing or with fewer numbers of channels. For example, for $N = 16$ channels, $\Delta f = 25$ GHz and $P_{\text{in}} = 8$ dBm, an increase in D from 5 to 10 (ps/nm)/km causes a reduction of the BER from 2×10^{-3} to 3.8×10^{-6}. So graphs like Figs. 6(a)–6(c) are useful in determining the maximum input power allowed in a WDM link, given its characteristics, i.e., channel spacing Δf, fiber dispersion coefficient D, and the total number of channels. For example, for $N = 32$, $D = 2$ (ps/nm)/km, and $\Delta f = 50$ GHz, the input power of each channel must not exceed 4.9 dBm if the BER is not to exceed 10^{-9}. Note that this result is obtained for a fiber length of $L = 80$ km. As the FWM influence is not much different in systems with fiber

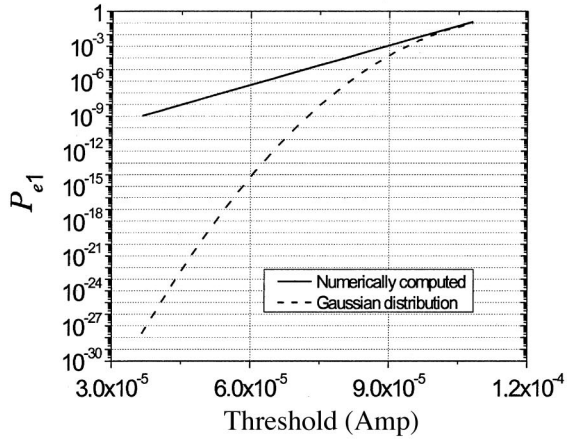

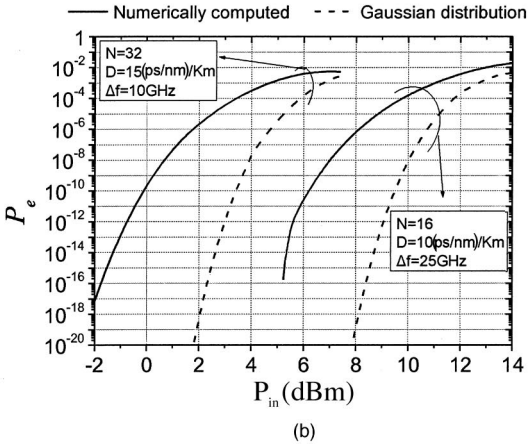

Fig. 4. (a) Error probability in the mark state with respect to the receiver threshold for $N = 16$, $D = 10$ (ps/nm)/km, $P_{\text{in}} = 5$ dBm, and $\Delta f = 25$ GHz for the Gaussian and numerical models. (b) BER dependence with respect to the input power for the Gaussian and the numerical models.

lengths longer than the effective length defined as $[1 - \exp(-aL)]/a$, these results are also valid when the total fiber length is longer than the effective length.

Note that the analysis carried out so far assumes a single-span system. If the system consists of multiple spans and if optical amplifiers are used to compensate for the optical losses, then additional FWM noise products are generated in each span. The phase of these products depends on the phase of the channels at the input of the span. It can be assumed[4] that the dispersion of each fiber span differs slightly and that the lengths of the fibers used in the span are different. Hence it is possible to assume that the phases of the channels at the beginning of each span are independent of one another. This implies that the phases of the products in different spans are independent as well. Also, the net dispersion in each span causes a walk-off of neighboring channels by at least one bit period. Hence the FWM noise products in each span can be assumed to be independent and the pdf of the total

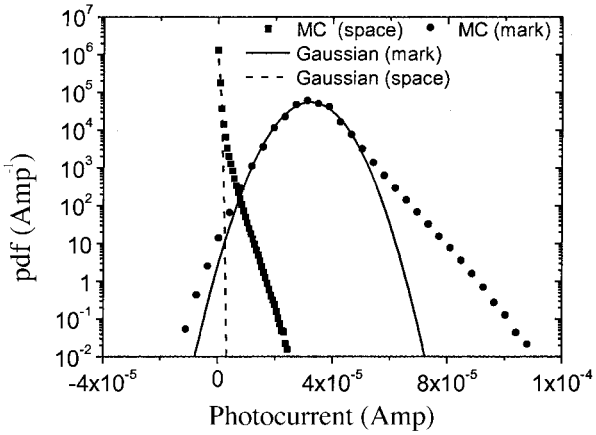

Fig. 5. Pdfs of the photocurrent in the mark and the space states for $N = 16$, $D = 0$ (ps/nm)/km, $dD/d\lambda = 0.07$ (ps/nm^2)/km, $P_{\text{in}} = 0$ dBm, and $\Delta f = 100$ GHz.

FWM noise can be approximated by the convolution of the individual FWM noise pdfs. These assumptions may not be valid in all cases. If for example, the dispersion is completely compensated for in each span; then the phases of the channels cannot be considered independent. In such cases one can compute, the pdfs of S_m and S_s by altering the FWM efficiency η in Eq. (4a) to take into account the number of spans as in Ref. 14. Doing so, however, prohibits the use of the auxiliary variables I_m and I_s whose applicability assumes the FWM efficiency given by Eq. (4a). Consequently the MC simulations must be performed again, this time for S_m and S_s directly.

6. Incorporation of Other Noises

In actual systems, receivers can suffer from other noises, such as thermal and ASE noise. To include these noises, one can use a technique based on the moment generating function (MGF) of the decision variable,[11,15] whereas the error probability can be estimated by use of the saddle-point approximation through the MGF.

To illustrate the above technique, we assume a simple optically preamplified receiver with a rectangular optical filter and an integrate-and-dump electrical filter. The MGF $M_Z(s)$ of decision variable Z at the receiver is defined as the expected value of e^{sZ}. Under the assumption that the quantum efficiency of the photodetector equals unity, the MGF $M_Z(s)$ of Z is related to the MGF $M_X(s)$ of the energy X of the incident optical field at the input of the amplifier through[15]

$$M_Z(s) = E[M_{Z|X}(s)] = \left(\frac{1}{1 - N_o s}\right)^{\mu} M_X\left(\frac{Gs}{1 - N_o s}\right). \tag{15}$$

In Eq. (15), $N_o = n_{\text{sp}}(G - 1)$ is the power spectral density of the ASE noise and G and n_{sp} are the gain and the spontaneous emission parameter of the optical amplifier, respectively. $\mu + 1$ is equal to the

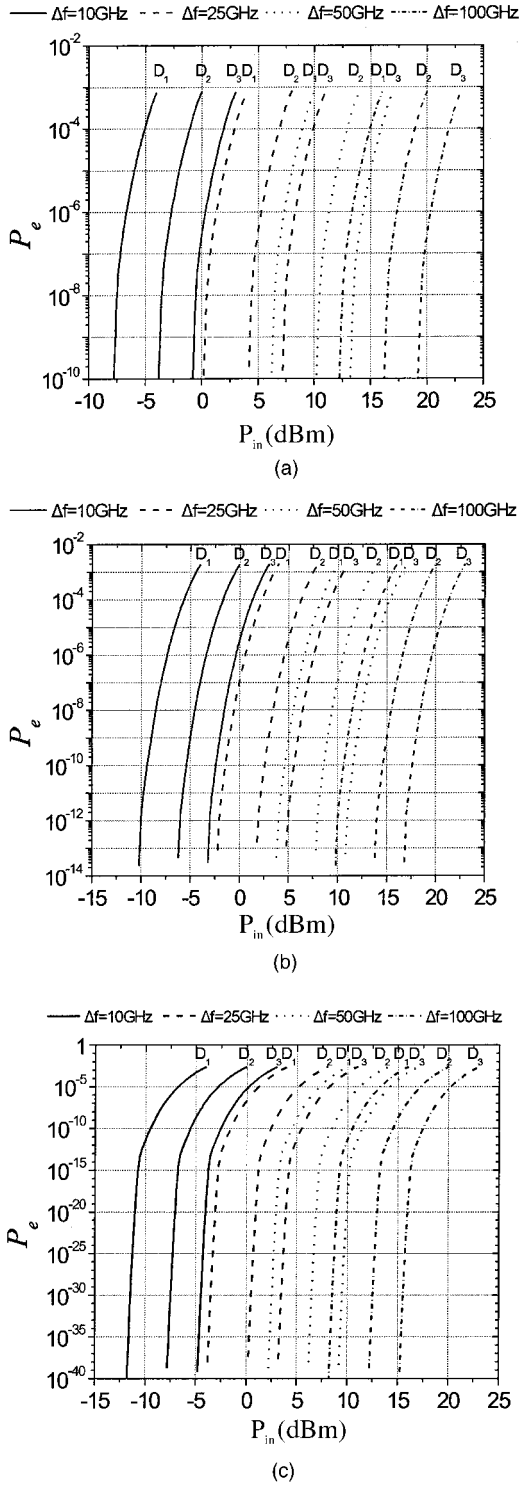

Fig. 6. BER as a function of input peak power P_{in} in the mark state for (a) $N = 8$, (b) $N = 16$, and (c) $N = 32$. The values of the chromatic dispersion used are $D_1 = 2$ (ps/nm)/km, $D_2 = 5$ (ps/nm)/km, and $D_3 = 10$ (ps/nm)/km.

product BT_b of bandwidth B of the optical filter and bit duration T_b (μ is assumed to be an integer). Hence the MGF of Z can be directly computed from the MGF of X by a simple change of variables and multiplication by $(1 - N_0 s)^{-\mu}$. Assuming rectangular pulses in all channels for the mark state, it is easy to show that $X = ST_b$, where $S = S^{(m)}$ and $S = S^{(s)}$ for the mark and the space states, respectively, of the central channel. To estimate the MGF of $X = ST_b$ one can use the approximate exponential formulas for the pdf of S. For example, in the space state where $X = k\delta^2 T_b I_s$, $M_X(s)$ is written approximately as

$$M_X(s) \cong \frac{A}{b + s'} \{\exp[(b + s')I_{s,\max}] - 1\}, \quad (16)$$

where $s' = k\delta^2 T_b$ and the exponential approximation Ae^{bx} for the pdf of I_s is used (Section 3). Note that one could obtain a more accurate estimation of the MGF of X by directly using the pdf computed from the MC simulations and numerical integration. Using Eq. (15) and expression (16) one can compute the MGF of the decision variable at the receiver, including the influence of the FWM and ASE noises. An expression similar to formula (16) can be derived for the mark state. To take into account the electrical thermal noise, we multiply the MGF of decision variable Z by $\exp(\sigma_{th}^2 s^2/2)$, which is the MGF of the thermal noise. The power of the thermal noise is equal to $\sigma_{th}^2 = 2K_B T_K T_b/(q^2 R_L)$, where K_B is Boltzmann's constant, R_L is the load resistor of the photodetector, T_K is the temperature (in degrees kelvin), and q is the charge of the electron. Using the above remarks, one can approximately compute the MGF of the decision variable and use the saddle-point approximation to estimate the error probabilities from the MGF.[11] Equation (15) also provides an indication of the validity of the Gaussian model for the description of the statistics of the decision variable in the presence of FWM and ASE noises. The shape of the MGF of Z is related to the respective shape of X, which, as indicated by formula (16), cannot be assumed Gaussian. Consequently, it is expected that the MGF of Z will also not be Gaussian, especially if the FWM noise (amplified by the optical amplifier) is dominant. This implies that the Gaussian model may not give accurate values for the error probability. However, if the receiver is dominated by the Gaussian distributed thermal noise (e.g., in the absence of optical preamplification), the pdf of the decision variable can be approximated accurately enough by a Gaussian distribution.

7. Conclusions

In this paper the statistical behavior of FWM noise has been investigated, and its implications in the performance of a WDM system were analyzed as well. Using numerical MC simulations, we have calculated the pdfs of the FWM noise in the space state for the first time to our knowledge. It was also shown both by MC simulations and by theoretical considerations that the pdf in the mark state is not symmetric as had previously been assumed in the literature. Hence the proposed model is considered more accurate than the models used so far. By fitting the data obtained from numerical simulations, approximate expressions of both pdfs were derived, and diagrams have

been given that allow the computation of these expressions, given the number of channels. With these diagrams, the pdfs can be estimated without the need to perform any MC simulations. The model was then used to estimate the performance of a WDM system for various values of its parameters (fiber dispersion, channel spacing and input power). The results obtained can be useful in the design of practical systems. A comparison of the present model and two models previously proposed was carried out, and it was shown that the previous models may not provide an accurate value for the BER. Finally, some guidelines for the incorporation of other noises (thermal and ASE) were presented.

Appendix A. Calculation of the Odd-Order Moments

In this appendix the first two odd-order moments $\langle I_m^{2u+1}\rangle$ of photocurrent I_m in the mark state are calculated. For $u = 0$, $\langle I_m^{2u+1}\rangle = \langle I_m\rangle$ is given by

$$\begin{aligned}\langle I_m\rangle &= \left\langle \frac{1}{3}\sum_{pqr} e_{pqr}\right\rangle = \left\langle \frac{1}{3}\sum_{pqr}\frac{d_{pqr}B_pB_qB_r}{|p-n\|q-n|}\right.\\ &\quad\left.\times\cos(\theta_{pqr}-\theta_n)\right\rangle\\ &= \frac{1}{3}\sum_{pqr}\left[\frac{d_{pqr}}{|p-n\|q-n|}\langle B_pB_qB_r\rangle\right.\\ &\quad\left.\times\langle\cos(\theta_{pqr}-\theta_n)\rangle\right] = 0 \qquad \text{(A1)}\end{aligned}$$

because $\langle\cos(\theta_{pqr}-\theta_n)\rangle = \langle\cos(\theta_p+\theta_q-\theta_r-\theta_n)\rangle = 0$. However, for $u = 1$, the third moment $\langle {I_m}^3\rangle$ of I_m is

$$\begin{aligned}\langle {I_m}^3\rangle &= \left\langle\left[\frac{1}{3}\sum_{pqr}\frac{d_{pqr}B_pB_qB_r}{|p-n\|q-n|}\cos(\theta_{pqr}-\theta_n)\right]^3\right\rangle\\ &= \left\langle\left(\frac{1}{3}\sum_{pqr}e_{pqr}\right)^3\right\rangle\\ &= \frac{1}{27}\left\langle\sum_{pqr}{e_{pqr}}^3\right\rangle + \frac{1}{9}\left\langle\sum_{pqr\neq p'q'r'}({e_{pqr}}^2e_{p'q'r'})\right\rangle\\ &\quad+\frac{2}{9}\left\langle\sum_{pqr\neq p'q'r'\neq p''q''r''}(e_{pqr}e_{p'q'r'}e_{p''q''r''})\right\rangle, \qquad \text{(A2)}\end{aligned}$$

where $e_{pqr} = d_{pqr}B_pB_qB_r\cos(\theta_{pqr}-\theta_n)/|p-n|/|q-n|$.

Using simple mathematical operations, one can show that the terms in the sums of (A2) have a mean value of either 1 or 0. Indeed, it is easy to show that every term of the sums of Eq. (A2) can be expanded into a linear superposition of terms of the type $\cos\theta = \cos(a_p\theta_p + a_q\theta_q + a_r\theta_r - a_n\theta_n + \ldots + a_{p''}\theta_{p''} + a_{q''}\theta_{q''} + a_{r''}\theta_{r''} + a_n\theta_{n''})$, whose mean value will be either 1 if $\theta \equiv 0$ or 0 if $\theta \neq 0$. The coefficient of every term of the above type in the superposition is positive. For example, working with the terms of the third sum of (A2), one can write

$$\begin{aligned}\theta &= \theta_{pqr-n} + \theta_{p'q'r'-n} - \theta_{p''q''r''-n}\\ &= \theta_p + \theta_q - \theta_r - \theta_n + \theta_{p'} + \theta_{q'} - \theta_{r'} - \theta_n - \theta_{p''} - \theta_{q''}\\ &\quad + \theta_{r''} + \theta_n. \qquad \text{(A3)}\end{aligned}$$

For the terms for which $r'' = n$, $p = r'$, $p' = r$, $q = p''$, and $q' = q''$, one obtains $\theta \equiv 0$. As $\theta \equiv 0$, one has $\langle\cos\theta\rangle = 1$, and the mean value of the corresponding terms will be 1. For the terms for which all the phases θ_i in θ do not cancel out ($\theta \neq 0$), θ will be given by a linear combination of the independent random variables θ_k, each of which is uniformly distributed in $[0, 2\pi]$, and hence $\langle\cos\theta\rangle = 0$. Therefore for these terms the mean value vanishes. From the above remarks one can easily conclude that $\langle {I_m}^3\rangle > 0$.

The authors thank George Kakaletris for his valuable programming assistance.

References

1. H. J. Thiele, R. I. Killey, and P. Bayvel, "Investigation of XPM distortion in transmission over installed fiber," IEEE Photon. Technol. Lett. **12,** 669–671 (2000).
2. M. Shtaif and M. Eiselt, "Analysis of intensity interference caused by cross-phase-modulation in dispersive optical fibers," IEEE Photon. Technol. Lett. **10,** 979–981 (1998).
3. K. Inoue, K. Nakanishi, K. Oda, and H. Toba, "Crosstalk and power penalty due to fiber four-wave mixing in multichannel transmissions," J. Lightwave Technol. **12,** 1423–1439 (1994).
4. M. Eiselt, "Limits on WDM systems due to four-wave mixing: a statistical approach," J. Lightwave Technol. **17,** 2261–2267 (1999).
5. J. G. Proakis, *Digital Communications*, 4th ed. (McGraw-Hill, New York, 2000).
6. K. Inoue, "Polarization effect on four-wave mixing efficiency in a single-mode fiber," IEEE J. Quantum Electron. **28,** 883–894 (1992).
7. N. Shibata, K. Nosu, K. Iwashita, and Y. Azuma, "Transmission limitations due to fiber nonlinearities in optical FDM systems," IEEE J. Sel. Area Commun. **8,** 1068–1077 (1990).
8. G. P. Agrawal, *Nonlinear Fiber Optics*, 2nd ed. (Academic, New York, 1995).
9. S. Song, C. T. Allen, K. R. Demarest, and R. Hui, "Intensity-dependent phase-matching effects on four-wave mixing in optical fibers," J. Lightwave Technol. **17,** 2285–2290 (1999).
10. K. O. Hill, D. C. Johnson, B. S. Kawasaki, and R. I. MacDonald, "cw three-wave mixing in single-mode optical fibers," J. Appl. Phys. **49,** 5098–5106 (1978).
11. G. H. Einarsson, *Principles of Lightwave Communications* (Wiley, Chichester, UK, 1996).
12. J. Tang, C. K. Siew, and L. Zhang, "Optical nonlinear effects on the performance of IP traffic over GMPLS-based DWDM networks," Computer Commun. **26,** 1330–1340 (2003).
13. P. E. Green, *Fiber Optic Networks* (Prentice-Hall, Englewood Cliffs, N.J., 1993).
14. K. Inoue, "Phase-mismatching characteristic of four-wave mixing in fiber lines with multistage optical amplifiers," Opt. Lett. **17,** 801–802 (1992).
15. T. Kamalakis and T. Sphicopoulos, "Asymptotic behavior of in-band crosstalk noise in WDM networks," IEEE Photon. Technol. Lett. **15,** 476–478 (2003).